Instability of converging shock waves and sonoluminescence

Allan K. Evans
Department of Mathematical Sciences, De Montfort University, The Gateway, Leicester LE1 9BH, United Kingdom
(Received 30 May 1996)

We study the problem of the stability of a nearly spherical converging shock wave in a van der Waals gas and consider the implications for sonoluminescence. An approximate geometrical theory of shock propogation, due to Whitham [*Linear and Non-linear Waves* (Wiley, New York, 1974); J. Fluid. Mech. **2**, 146 (1957); **5**, 369 (1959)], is used. A first-order treatment of deviations from spherical symmetry, similar to one performed by Gardner, Brook, and Bernstein [J. Fluid Mech. **114**, 41 (1982)] for an ideal gas, shows that these deviations are unstable, coming to dominate the shape of a shock wave as it converges. The instability is weak, although not as weak as in an ideal gas. Perturbations grow as a small inverse power of the radius. The mechanism for concentration of energy in sonoluminescence involves a spherical converging shock. The validity of the theory given here is checked by comparing the results for spherically symmetric shocks with a simulation by Kondic, Gersten, and Yuan [Phys. Rev. E **52**, 4976 (1995)]. We then estimate the degree of bubble symmetry necessary for sonoluminescence and relate this result to the experimental robustness of sonoluminescence. [S1063-651X(96)01211-1]

PACS number(s): 47.40.−x, 78.60.Mq, 62.50.+p

I. INTRODUCTION

Sonoluminescence [1,2] is a remarkable phenomenon where a small bubble of gas, surrounded by liquid, collapses so quickly that the gas inside the bubble is heated to a temperature where it emits light. The energy for this collapse is supplied by sound waves in the surrounding liquid. Water is the most commonly used liquid, and most experiments have used bubbles of air, although various other gases such as hydrogen [3] and ethane [4] have been successfully used. A recent series of elegant experiments by Putterman and coworkers [3–7] has explored the dependence of sonoluminescence on the composition of the fluids and on the various control parameters.

Although it has recently been suggested that sonoluminescence is caused by a quantum radiation effect [8], this theory is unproven. In this paper we take the more conventional view that light emission is due to a hot spot at the center of the bubble. Energy is concentrated first by a collapsing bubble and then by a shock wave, launched towards the bubble's center as the bubble nears its minimum radius. This theory, proposed by Greenspan and Nadim [9], explains the very short duration of the pulses of light observed in sonoluminescence, as well as the high temperatures necessary for light emission.

A critical feature of sonoluminescence is the spherical symmetry of the bubble. Only if the collapsing bubble is nearly spherical can a shock wave focus accurately at the very center of the bubble, producing very high temperatures. However, theoretical studies [9–13] have largely ignored deviations from spherical symmetry because of the difficulty of fully three-dimensional calculations. Some authors, most notably Brenner *et al.* [14,15] and Lofstedt *et al.* [17] have recently considered deviations from symmetry in the bubble surface, but no three-dimensional study of the dynamics of the gas enclosed in the bubble has been attempted. In this paper, we study the three-dimensional dynamics of shocks inside the bubble.

The assumption of complete spherical symmetry greatly simplifies calculations, but removes some important physical effects. The size of deviations from spherical symmetry controls how sharply the converging shock wave focuses and so may limit the maximum temperature reached. Deviations from spherical symmetry must also play an important role in the differences between multibubble and single-bubble sonoluminescence [16]. Experiments [7] show an abrupt cessation of the nonspherical oscillations of a bubble as sonoluminescence begins. This transition is one of the most mysterious features of sonoluminescence [17].

The subject of the present paper is the propagation of deviations from spherical symmetry in a strong near-spherical shock wave as it converges in a van der Waals gas. We use an approximate, geometrical theory of shock wave propagation, due to Whitham [18], and a further approximation valid for strong shocks. The geometrical theory is well adapted to converging shock waves and gives highly accurate results in the case of spherical symmetry. Since a converging shock is strengthened as it focuses on the origin, the strong-shock approximation is appropriate. The same approximations were used by Gardner *et al.* [19] in their analysis of shock convergence in an ideal gas.

The behavior of converging shocks in ideal gases has been studied in some depth using the geometrical theory. It is well known [18] that plane shock waves are stable, in the sense that small deviations from the planar shape are reduced in size as the shock propagates, and that cylindrical converging shocks are unstable. These results are valid only in the linear approximation and do not apply to large deviations from spherical or cylindrical symmetry. Numerical analysis of the equations of shock dynamics shows that in the two-dimensional case, polygonal converging shocks may be stable and produce the same energy concentration as cylindrically symmetric shocks [20].

In the spherical case, Gardner *et al.* [19] have analyzed the stability of converging spherical shocks in an ideal gas in the linear approximation, using a different formulation of the

theory of shock dynamics to the one we employ. They found a weak instability. The numerical results of Schwendeman confirm this conclusion [21].

We shall see that the additional terms in the van der Waals equation of state modify the results only by changing the value of some exponents: the qualitative behavior is the same as for an ideal gas. Hence small deformations of a converging spherical shock in a van der Waals gas are unstable: they come to dominate the shape of the shock wave as it converges. However, the instability is weak. Deformations grow only as a small inverse power of the radius, although the growth is faster than in an ideal gas. The weakness of the instability helps to explain the robustness of sonoluminescence as an experimental phenomenon.

In the final part of the paper, the implications of the results for sonoluminescence are discussed. We estimate the degree of bubble symmetry necessary for sonoluminescence and some possible sources of deviations from spherical symmetry, including thermal fluctuations, are considered.

The physical quantities used in this paper are those for a bubble of air in water. Where detailed knowledge of the dynamics of a sonoluminescing bubble is necessary, we use the results of the recent simulations by Kondic *et al.* [12].

II. DYNAMICS OF CONVERGING SHOCKS

We now present a simple theoretical treatment of instabilities in a strong, converging spherical shock in a van der Waals gas. In Sec. II A, we describe the equation of state and notation used. In Sec. II B, shock equations for strong shocks are derived. The approximate theory of shock propagation is then described in Secs. II C 1 and II C 2. We apply this theory, first, in Sec. II D 1, to a spherically symmetric shock and then, in Sec. II D 2, to deviations from spherical symmetry.

A. The van der Waals gas

Because of the high pressures reached when the bubble is at its smallest, we use the van der Waals equation of state [22] with no attraction term. Written in terms of the density $\rho = 1/V$, the equation is

$$p = \frac{RT}{1/\rho - b}. \tag{1}$$

The excluded volume is $b = 1.26 \times 10^{-3}\ \mathrm{m^3\ kg^{-1}}$ and R is the gas constant per kilogram, $R = 285\ \mathrm{J\ kg^{-1}\ K^{-1}}$. The maximum possible density is

$$\rho_m = \frac{1}{b} = 794\ \mathrm{kg\ m^{-3}}. \tag{2}$$

The same equation of state was used by Wu and Roberts [11] and by Kondic *et al.* [12] in their numerical calculations.

We introduce the parameters

$$z = 1 - b\rho \tag{3}$$

and

$$y = 1 - \frac{b\rho}{\gamma}, \tag{4}$$

so that setting $y = z = 1$ recovers the ideal gas equations. The van der Waals equation then becomes

$$\frac{p}{\rho} = \frac{RT}{z}. \tag{5}$$

Since the entropy of the van der Waals gas is [22]

$$S = c_v \ln[p(V-b)^\gamma] + \text{ const}, \tag{6}$$

the speed of sound a, which satisfies

$$a^2 = \left|\frac{\partial p}{\partial \rho}\right|_S, \tag{7}$$

is given by

$$a^2 = \frac{\gamma p}{\rho z}. \tag{8}$$

We shall also use the enthalpy

$$h = \frac{p}{\rho}\frac{\gamma y}{\gamma - 1}. \tag{9}$$

B. Shock equations for strong shocks

Three equations relating the fluid-mechanical quantities on either side of a shock wave can be derived from the conservation of energy, momentum, and mass [18]. They are

$$\rho_2 v_2 = \rho_1 v_1, \tag{10}$$

$$p_2 + \rho_2 v_2^2 = p_1 + \rho_1 v_1^2, \tag{11}$$

and

$$h_2 + \tfrac{1}{2} v_2^2 = h_1 + \tfrac{1}{2} v_1^2. \tag{12}$$

In these equations, the subscript 1 denotes variables ahead of the moving shock front and the subscript 2 variables behind the front. The velocities v_1 and v_2 are measured in the frame of reference where the shock is stationary.

We shall now derive ''shock conditions'' for strong shocks in the van der Waals gas. These are equations that relate the temperature, pressure, and density behind a strong shock to the Mach number of the shock and the state of the gas in the undisturbed area ahead of the shock. The Mach number M is the speed of the shock relative to the gas ahead, measured in units of the sound speed. Therefore

$$v_1 = M a_1 \tag{13}$$

and

$$v_1^2 = M^2 a_1^2 = \frac{M^2 \gamma p_1}{\rho_1 z_1}. \tag{14}$$

Eliminating v_2 from Eqs. (10)–(12) and then replacing v_1 using Eq. (14) yields

$$\frac{p_2}{p_1}=1+\frac{\gamma M^2}{z_1}\left(1-\frac{1}{\mu}\right) \tag{15}$$

and

$$\frac{p_2}{p_1}\gamma y_2-\mu\gamma y_1=\frac{\gamma(\gamma-1)\mu M^2}{2z_1}\left(1-\frac{1}{\mu^2}\right), \tag{16}$$

where $\mu=\rho_2/\rho_1$. Eliminating p_2/p_1, we obtain

$$M^2(\mu-1)[(\gamma-1)(\mu+1)-2y_2\gamma]+2\mu z_1(\mu y_1-y_2)=0. \tag{17}$$

To find the limiting condition for strong shocks, we take the limit $M\to\infty$, obtaining a quadratic equation in μ:

$$\mu^2(\gamma-1)-2\gamma y_2\mu+\gamma(2y_2-1)+1=0. \tag{18}$$

The two solutions are $\mu=1$, which corresponds to the situation where no shock is present, and

$$\mu=\frac{\gamma+1}{\gamma-1}-\frac{2b\rho_2}{\gamma-1}. \tag{19}$$

Since $\mu=\rho_2/\rho_1$, this gives us the density behind the shock in terms of the density ahead:

$$\rho_2=\frac{(\gamma+1)\rho_1}{\gamma-1+2b\rho_1}. \tag{20}$$

This is the first of the shock conditions. We can obtain similar Eqs. for p_2 and v_2: eliminating μ from Eqs. (15) and (19) gives

$$p_2=\frac{2\gamma M^2 p_1}{\gamma+1} \tag{21}$$

and using Eqs. (10) and (19) gives

$$v_2=a_1 M\frac{\gamma-1+2b\rho_1}{\gamma+1}. \tag{22}$$

We shall also need the absolute velocity of the gas behind the shock, assuming that the gas in front is stationary. This is

$$u_2=a_1 M-v_2=\frac{2a_1 M z_1}{\gamma+1}. \tag{23}$$

Eqs. (20)–(23) reduce to the equations for an ideal gas [see [18], Eq. (6.110)] when $z_1=y_1=1$. We shall also use an equation for the value of a behind the shock:

$$a_1^2=\frac{2\gamma}{\gamma-1}\left[\frac{a_1 M}{\gamma+1}(\gamma-1+2b\rho_0)\right]^2. \tag{24}$$

C. Shock dynamics

In this section, we describe an approximate theory of shock wave propagation, due to Whitham. The theory is described in detail in Whitham's book [18] and in the original papers [23,24]. Here we give a brief summary and note the minor changes that are necessary when the van der Waals equation of state is used rather than the ideal gas equation. The theory will be used in the next section to treat asymmetries in imploding shock waves.

1. The Chisnell-Whitham characteristic rule

The starting point for the theory is the application of the equations of gas dynamics to the problem of shock propagation down a tube of nonuniform cross section $A(x)$. By averaging the gas equations across the tube [18], we obtain

$$\rho_t+u\rho_x+\rho u_x+\frac{\rho u}{A}\frac{dA}{dx}=0, \tag{25}$$

$$\rho(u_t+uu_x)+p_x=0, \tag{26}$$

$$p_t+up_x-a^2(\rho_t+u\rho_x)=0, \tag{27}$$

where subscripts denote partial derivatives.

A natural approach to the solution of these equations is to use the method of characteristics. One of the characteristic equations is

$$\frac{dp}{dx}+\rho a\frac{du}{dx}+\frac{\rho a^2 u}{(u+a)A}\frac{dA}{dx}=0, \tag{28}$$

which applies to the characteristic

$$\frac{dx}{dt}=\rho(u+a). \tag{29}$$

Equation (28) is valid only along the curves in the (x,t) plane, behind the shock front, described by (29). The idea of the Chisnell-Whitham characteristic rule is to apply (28) *along* the shock front. We thus neglect the difference in the constants of integration obtained when (28) is solved on different characteristics that intersect the shock front. These differences arise from the nonuniformity of the flow behind the shock, so the characteristic rule effectively ignores the influence of the flow behind the shock wave on the shock propagation. Whitham [18,23,24] discusses the error introduced by this approximation. Because the effect of the flow behind the shock on the shock dynamics is ignored, the approximation is very good for situations where the shock wave accelerates with time, so that features of the flow behind do not ''catch up'' with the shock. The best examples of flows with this characteristic are converging shock waves, which are the subject of this paper. For spherically and cylindrically symmetric implosions in ideal gases, the results of the Chisnell-Whitham rule can be compared with exact solutions and are correct to three significant figures.

Assuming that the characteristic equation (28) applies on the shock front, we can use the shock conditions (20)–(24) to write the quantities in it, which are those immediately behind the shock, in terms of those ahead of the shock and the Mach number. The shock conditions we use here are the strong shock conditions for the van der Waals gas rather than the ideal gas shock conditions used by Whitham [18]. The result is

$$\frac{\lambda}{M}\frac{dM}{dx}+\frac{1}{A}\frac{dA}{dx}=0, \tag{30}$$

where

$$\lambda = 1 + \frac{2(\gamma-1)}{\gamma\omega_1} + \frac{\gamma+2b\rho_1}{\omega_1}\left(\frac{2(\gamma-1)}{\gamma}\right)^{1/2} \tag{31}$$

and

$$\omega_1 = \gamma - 1 + 2b\rho_1 . \tag{32}$$

For $b=0$, this reduces to the value for strong shocks in the ideal gas, as calculated by Whitham [18]:

$$\lambda = 1 + \frac{2}{\gamma} + \left(\frac{2\gamma}{\gamma-1}\right)^{1/2} . \tag{33}$$

The differential equation (30) can easily be solved to give A as a function of the Mach number M:

$$M = M_0 A^{-\lambda} . \tag{34}$$

This equation, valid for strong shocks in the van der Waals gas, is the main result of the Chisnell-Whitham rule.

2. The ray-tube approximation

The ray-tube approximation is used to construct an approximate geometrical theory of shock-wave motion. Each small element of a shock front is treated as if it were propagating in a tube whose walls are perpendicular to the shock front. This approximation is independent of the Chisnell-Whitham rule. Whitham [18,23,24] and others [19–21] have applied the theory produced by combining the two approximations to a variety of problems of shock diffraction and stability, and where the results can be compared with exact theoretical results or with experiment, the theory proves very accurate.

The theory is formulated in terms of a function $\alpha(\mathbf{x})$ whose contours give the positions of the shock front at different times. The solution of the equation

$$\alpha(\mathbf{x}) = a_1 t \tag{35}$$

is a surface that is the position of the shock at time t. The function $\alpha(\mathbf{x})$ therefore defines the trajectory of the shock front completely. Whitham [18] shows that the geometry of ray tubes implies that $\alpha(\mathbf{x})$ satisfies the equations

$$M = \frac{1}{|\nabla\alpha|} \tag{36}$$

and

$$\nabla\cdot\left(\frac{M}{A}\nabla\alpha\right) = 0. \tag{37}$$

We shall refer to these two equations as the Whitham equations. Together with the relationship between M and A [Eq. (34)], they form the basis of the geometrical theory of shock propagation. Using the equations in this form, rather than in the form used by Gardner *et al.* [19], will allow us to perform the stability calculation simply.

D. Converging shock waves

We now apply the geometrical theory of shock dynamics to the problem of converging shock waves. The first step is to find the solution of the geometrical shock equations that corresponds to a spherically symmetric converging shock. This solution is well known [18] and provides a simple example of the use of the equations. It will be used as the starting point for the perturbation theory of the following section, where deviations from the spherical solution are treated.

1. Spherically symmetric converging shocks

We assume $\alpha = \alpha(r)$, where r is the distance from the origin, and also $A = A(r)$ and $M = M(r)$. We then have

$$\nabla\alpha = \hat{\mathbf{r}}\frac{d\alpha}{dr} . \tag{38}$$

For a shock moving inward, $d\alpha/dr < 0$, so the first Whitham equation (36) gives

$$M = -\left(\frac{d\alpha}{dr}\right)^{-1} \tag{39}$$

and the second (37) becomes

$$\nabla\cdot\left(\frac{\hat{\mathbf{r}}}{A}\right) = 0. \tag{40}$$

The vector field $\hat{\mathbf{r}}/A$ is therefore conservative and the only possible choice is

$$A = A_0 r^2 , \tag{41}$$

where A_0 is a constant. This is exactly as we would expect: A is simply the area available for shock propagation at radius r.

Now that we have the form of $A(r)$, the relationship (34) between M and A gives us $M(r)$:

$$M = \frac{1}{\beta} r^{-2/\lambda} , \tag{42}$$

where β is a constant. The function $\alpha(r)$ can be obtained by solving the differential equation (39). The result is

$$\alpha(r) = -\frac{\beta}{1+2/\lambda} r^{1+2/\lambda} . \tag{43}$$

The constant of integration has been chosen so that the time when the shock wave reaches the origin is $t=0$. Since $\alpha(r) = a_1 t$, the radius as a function of time is

$$r = r_0(-t)^{\lambda/(\lambda+2)} , \tag{44}$$

where r_0 is a constant.

For an ideal gas with $\gamma = 1.4$, we have $\lambda = 5.0743$, and the exponent for the Mach number in Eq. (42) is $2/\lambda = 0.3943$, agreeing with the exact result from the solution of Guderley [18,25] to three significant figures. The accuracy of this approximate theory for an unperturbed spherical shock in an ideal gas is therefore excellent.

The numerical results of Kondic *et al.* [12], giving the trajectory of a spherically symmetric shock wave in a collapsing bubble, can also be compared with the above result.

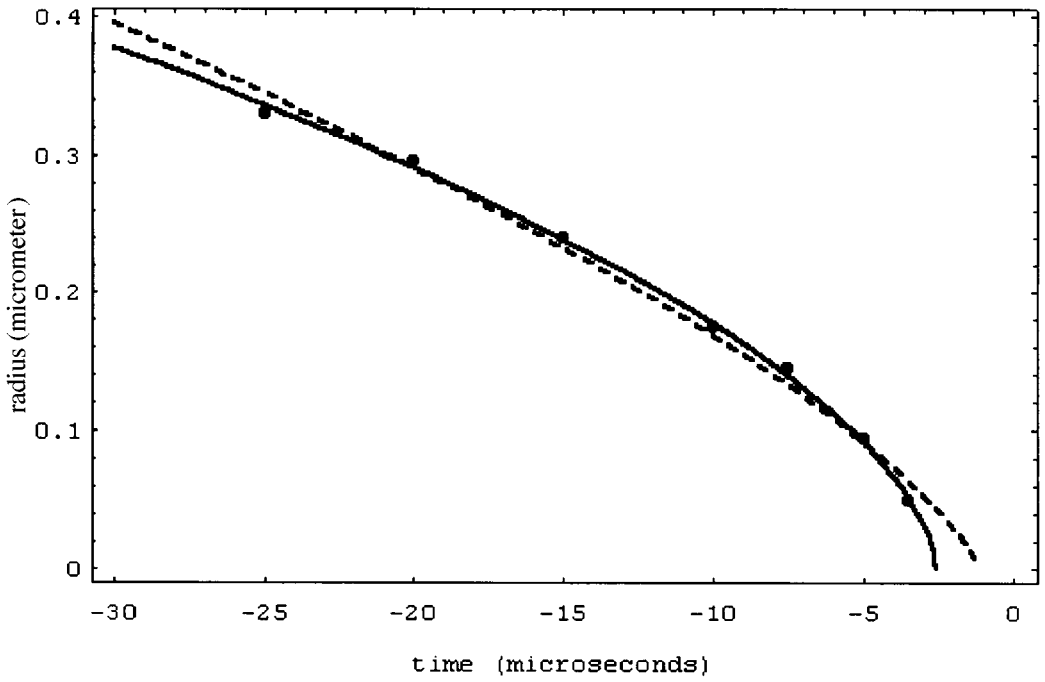

FIG. 1. Trajectories of spherical converging shock waves from the approximate theory of shock propagation and from the numerical simulation of Kondic *et al.* [12]. The dots are points taken from a graph in the paper of Kondic *et al.*, the dotted line is calculated from the theoretical trajectory for an ideal gas, and the solid line is from the theoretical trajectory for a van der Waals gas.

For this we need the density ρ_1 of undisturbed gas ahead of the shock wave. The shock wave inside a sonoluminescing bubble is launched and converges while the bubble is close to its minimum radius. In the paper of Kondic *et al.*, this minimum radius is approximately 0.56 μm. The equilibrium radius of the bubble at atmospheric pressure is 4 μm, so assuming a density of 1.3 kg m^{-3} for air at 1 atm, we obtain a density for the gas in the bubble at minimum radius of $\rho_1 = 473$ kg m^{-3}. Equation (31) then yields $\lambda = 2.58$, and so the exponent in Eq. (44) that describes the time dependence of the shock's radius is

$$\frac{\lambda}{\lambda+2} = 0.56. \tag{45}$$

Using the parameters for an ideal gas gives the value 0.72. Figure 1 compares shock trajectories with these two exponents with data taken from a graph in the paper of Kondic *et al.* [12]. One can see that the theoretical curve for the van der Waals gas fits the data from the simulation very well. This agreement gives us some confidence that the approximate theory of shock propagation is valid for this problem.

2. Deviations from spherical symmetry

In this section, first-order perturbation theory is used to study the behavior of small deviations from the perfectly spherical shape of the preceding section. We aim to find out whether such perturbations become more or less important as the shock converges and to estimate their growth or decay rates. The treatment given here is essentially equivalent to that of Gardner *et al.* [19], although a different form of the Whitham equations is used.

We take

$$\alpha(r,\theta,\phi) = -\alpha_0(r) + \epsilon\mu(r)Y(\theta,\phi). \tag{46}$$

The term α_0 is the spherical solution as in Eq. (43) and the second term is a perturbation whose dependence on the radius is contained in the function μ. A suitable choice for $Y(\theta,\phi)$ is a spherical harmonic

$$Y(\theta,\phi) = P_n^m(\theta)\cos m\phi, \tag{47}$$

where $P_n^m(\theta)$ is an associated Legendre polynomial [26]. All calculations will be to first order in the perturbation parameter ϵ.

By placing this trial solution in the Whitham equations (36) and (37) and using the relationship (34) between M and A from the Chisnell-Whitham rule, we shall find the form of the function μ. We first calculate $\nabla\alpha$ to first order in ϵ:

$$\nabla\alpha = -\hat{\mathbf{r}}\beta r^{2/\lambda} + \epsilon\left[\hat{\mathbf{r}}\mu_r Y + \hat{\boldsymbol{\theta}}\frac{\mu Y_\theta}{r} + \hat{\boldsymbol{\phi}}\frac{\mu Y_\phi}{r\sin\theta}\right] + O(\epsilon^2). \tag{48}$$

As before, subscripts are used to denote partial derivatives. Using the first Whitham equation (36) and the relationship between M and A [Eq. (34)], we find that

$$\frac{M}{A} = M\left(\frac{M}{M_0}\right)^\lambda = \frac{1}{M_0^\lambda}|\nabla\alpha|^{-(1+\lambda)}. \tag{49}$$

Hence

$$\frac{M}{A} = \frac{1}{M_0^\lambda\beta^{1+\lambda}r^{2\lambda+2}}\left(1+\epsilon(1+\lambda)\frac{\mu_r Y}{\beta r^{2/\lambda}}\right) + O(\epsilon^2) \tag{50}$$

We now calculate $(M/A)\nabla\alpha$ by multiplying Eq. (50) by Eq. (48). Setting the divergence of this quantity to zero, as in the second Whitham equation (37), yields the partial differential equation

$$Y\sin\theta(2\mu_r r-\lambda\mu_{rr}r^2)+\mu\left(\frac{\partial}{\partial\theta}(Y_\theta\sin\theta)+\frac{Y_{\phi\phi}}{\sin\theta}\right)=0. \tag{51}$$

Since $P_n^m(\theta)$ obeys the associated Legendre equation [26], choosing Y as in Eq. (47) leads to an ordinary differential equation for μ:

$$\lambda r^2\frac{d^2\mu}{dr^2}-2r\frac{d\mu}{dr}+\mu n(n+1)=0. \tag{52}$$

This equation has solutions

$$\mu(r)=r^\xi, \tag{53}$$

where

$$\xi=\frac{1}{2\lambda}[2+\lambda\pm\sqrt{(2+\lambda)^2-4\lambda n(n+1)}]. \tag{54}$$

We now have the first-order behavior of $\alpha(r,\theta,\phi)$, but this is not the same as the position of the shock $r(\theta,\phi,t)$. The first-order term in r is related to the term in α by the equation

$$\delta r=-\delta\alpha\left(\frac{\partial\alpha_0}{\partial r}\right)^{-1}, \tag{55}$$

where $\alpha_0(r)$ is given by Eq. (43). Hence, if the perturbation to α is proportional to r^ξ, as in Eq. (53), the perturbation to r is proportional to r^χ, where

$$\chi=\xi-\frac{2}{\lambda}. \tag{56}$$

The $n=0$ spherical harmonics are independent of θ and ϕ. The first nontrivial solutions are those with $n=1$, but these represent translational motions of the bubble. Solutions for $n\geq 2$ represent true deformations of the shock's shape. Figure 2 shows the deformations of a sphere represented by the three $n=2$ spherical harmonics.

For $n\geq 2$, the discriminant in Eq. (54) is imaginary. The imaginary component of χ represents oscillations in the perturbations from spherical symmetry as the shock converges. The frequency of these oscillations depends on n (and on the radius r), but the rate of growth of the perturbation is independent of n for $n\geq 2$. The perturbations' dependence on r can be written as

$$\delta r\sim r^\chi=r^{\chi'}\cos\left(\frac{\ln r}{2\lambda}[(\lambda+2)^2-4\lambda n(n+1)]^{1/2}\right), \tag{57}$$

where χ' is the real part of χ,

$$\chi'=\frac{1}{2}-\frac{1}{\lambda}. \tag{58}$$

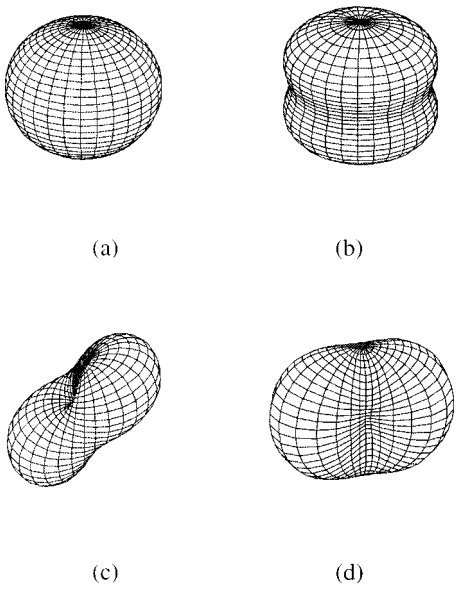

FIG. 2. Deformations of a sphere represented by the $n=2$ spherical harmonics. An undeformed sphere is shown in (a). Spherical harmonics Y_2^0, Y_2^1, and Y_2^2 are shown in (b), (c), and (d), respectively.

A measure of the influence of a perturbation on the shape of a nearly spherical shock wave is the size of the perturbation divided by the radius $\delta r/r$. Although the size δr of a perturbation decreases (as r^χ) as the shock converges, its influence on the shape of the shock increases (as $r^{\chi-1}$). Figure 3 shows the growth and oscillation of $\delta r/r$ for perturbations with $n=2$, 4, and 8. Both the magnitude and the frequency of oscillation of deformations of the spherical shock wave increase as the shock converges. The growth rate of perturbations is independent of the value of n, but perturbations with larger values of n oscillate more quickly.

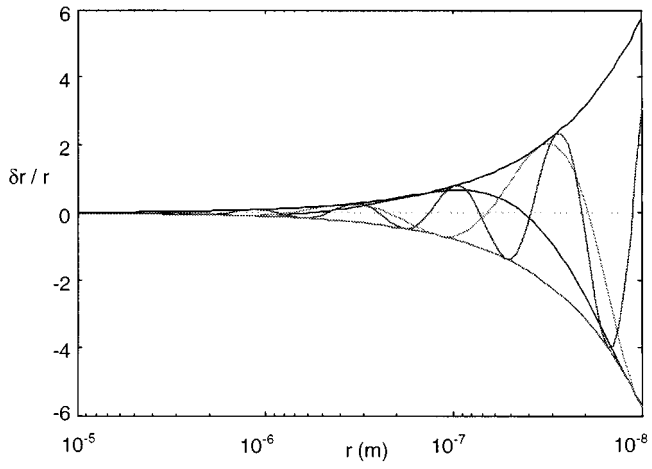

FIG. 3. Growth and oscillation of deformations of a spherical converging shock wave. The graph shows $\delta r/r$ for deformations from spherical symmetry described by spherical harmonics with $n=2$, 4, and 8. Perturbations with a larger value of n oscillate more quickly as the shock converges. However, the growth rate of perturbations is independent of n. The ''envelope'' curve that gives the amplitude of oscillations for all values of n is also shown.

We have shown that a collapsing spherical shock wave is unstable, but the instability is very weak. Perturbations grow as a power of the radius, rather than exponentially. A power-law instability of this kind also appears in the dynamics of the bubble surface [27]. Because the instability is weak, a collapsing shock that is nearly spherical is not always disrupted by instability before the collapse reaches very small scales. A certain size of deviation from spherical symmetry in the initial conditions is needed before the effects of the instability become large enough to be important.

III. DEVIATIONS FROM SPHERICAL SYMMETRY AND SONOLUMINESCENCE

In this section, we apply the results on the instability of converging shocks, obtained in the preceding section, to the theory of sonoluminescence. The high temperatures necessary for sonoluminescence are caused by a converging spherical shock. If this shock is disrupted by instability before it has time to concentrate energy at the center of the bubble, no light will be produced. We first estimate the size of the deviation from spherical symmetry in a collapsing bubble that is needed to disrupt sonoluminescence, then consider some possible sources of this asymmetry.

The physical parameters used are taken from the paper of Kondic *et al.* [12], which is the most recent and complete numerical simulation of sonoluminescence known to the author. The main physical assumption is that the linear theory of deviations from spherical symmetry remains approximately valid when deviations from spherical symmetry become large. Numerical evidence from the case of the ideal gas [20,21] suggests that any error in the linear approximation overestimates the rate of growth of large deviations. We can therefore regard the results of this section as an upper bound on the effect of shock instability.

A. Amount of distortion of a collapsing bubble necessary to inhibit sonoluminescence

The results of Kondic *et al.* [12] show that most of the light produced in a sonoluminescing bubble comes from a small volume, of radius $r_s \sim 10$ nm at the center of the bubble. If the converging shock wave is disrupted before it reaches this radius, sonoluminescence will not occur. The shock is disrupted if the size of perturbations from spherical symmetry at this point δr_s is of the same order as the radius r_s, that is, if

$$\frac{\delta r_s}{r_s} \sim 1. \tag{59}$$

To estimate the conditions that will bring about this asymmetry, we first need to calculate the exponent χ'. The value of λ derived from the results of Kondic *et al.* in Sec. II D 1. of the present paper is $\lambda = 2.59$, and so the exponent that describes the dependence of the shock's shape on radius is given by Eqs. (54) and (56) as

$$\chi' = \frac{1}{2} - \frac{1}{\lambda} = 0.11. \tag{60}$$

For an ideal gas $\lambda = 5.07$ and so the exponent χ' is 0.30. Perturbations are therefore more unstable in the van der Waals gas at this density than in the ideal gas.

In the calculations of Kondic *et al.*, the shock wave first appears at a radius r_l of around 0.36 μm. Since δr is proportional to $r^{\chi'}$, we have

$$\frac{\delta r_s}{r_s} \simeq \frac{\delta r_l}{r_l} \left(\frac{r_s}{r_l} \right)^{\chi' - 1}, \tag{61}$$

where δr_l is the size of the deviation from spherical symmetry at the point where the shock wave first appears. Setting $\delta r_s / r_s = 1$, we obtain a value for the size of perturbation at the launch of the shock that is required to disrupt sonoluminescence:

$$\delta r_l \sim 15 \text{ nm}, \tag{62}$$

or about 1/24 the radius of the shock wave. This illustrates the weakness of the shock wave's instability: a deformation of the shock's shape is magnified only by a factor of 24 as the shock wave itself collapses by a factor of 36.

The next question that must be considered is how asymmetries in the surface of a collapsing bubble are transmitted to the shock wave at its time of launch. The shock wave does not appear immediately inside the bubble surface. As the theory of Greenspan and Nadim [9] suggests and the simulations of Kondic *et al.* [12] show, a shock wave first appears when the bubble radius is nearing its minimum, at a distance from the bubble's center around two-thirds of the bubble radius. This means that there is a layer of gas between the bubble surface and the shock, which may smooth out some deviations from spherical symmetry, making the shock wave more symmetric than the bubble surface.

This effect will be much more pronounced for short-wavelength perturbations of the bubble surface (corresponding to spherical harmonics with large values of n) than it is for the long-wavelength perturbations (small values of n). For the lowest spherical harmonics, with $n = 2,3$, the effect will be relatively small, as pressure waves would need to travel around the inside of the bubble at very high speeds to smooth asymmetries of this wavelength. In the future we hope to develop a consistent theory of the interaction between deviations from spherical symmetry in the bubble and in the shock. For the approximate calculations presented here, we concentrate on long-wavelength modes and ignore this effect, while keeping in mind the possible error caused. We therefore estimate the amount of asymmetry in the bubble surface needed to disrupt sonoluminescence to be about one part in twenty.

B. Causes of asymmetry in the bubble surface

We now consider the possible sources of asymmetry in the collapsing bubble. The non-uniformity of the sound pressure field in the liquid surrounding the bubble can be ignored, since the wavelength of the sound is at least a few centimeters, while the size of the bubble is measured in micrometers. The next cause to consider is thermal fluctuations of the bubble.

The restoring force that controls thermal fluctuations of the bubble's surface is surface tension. For an order-of-

magnitude estimate, we take the increase in area of the bubble's surface due to a fluctuation in radius δr to be of order $(\delta r)^2$, giving a surface energy $E=\sigma(\delta r)^2$. The equipartition theorem then gives an estimate for the rms fluctuations:

$$\delta r_{\rm rms}\sim\left(\frac{kT}{\sigma}\right)^{1/2}. \tag{63}$$

For temperatures of a few thousand degrees kelvin, $\delta r_{\rm rms}\sim 1$ nm. Thermal fluctuations are therefore much too small to disrupt sonoluminescence. A more careful treatment, expanding the deviations from spherical symmetry in spherical harmonics, gives a similar result.

To understand how sonoluminescence is inhibited in certain parameter ranges in experiments, we must study the dynamics of the shape of a collapsing bubble, as in the theoretical work of Brenner *et al.* [14,15]. The subject is complicated by the presence of two different instabilities of the bubble surface and also by mass transport across the bubble surface, which is not well understood [15,17]. Neither theoretical studies of bubble dynamics nor experiments have yet yielded estimates of the size of deviations from spherical symmetry. However, Putterman and his group [28] are working on experiments to answer this question, and their preliminary results seem to indicate that the asymmetry in a collapsing bubble is of the same order of magnitude as the critical amount of asymmetry derived here.

IV. CONCLUSION

We have shown that in a van der Waals gas, small deformations of a nearly spherical converging shock wave increase as the shock converges. This suggests that at some critical radius, the spherical shape will be completely lost and the convergence disrupted. In this sense, a converging shock wave is unstable. The instability is weak, although not as weak as in an ideal gas. Perturbations to the spherical shape grow slowly, as an inverse power of the radius. In a sonoluminescing bubble of gas, this weakness is vitally important because it allows shock waves to focus energy in a very small region at the center of a bubble, even when slight deviations from spherical symmetry exist.

The conclusions reached here seem to depend on the assumption that the linear theory can be extended beyond its range of validity to large deviations from spherical symmetry. However, as we noted earlier, numerical evidence [20,21] suggests that any error in the linear theory overestimates the growth of large deviations. Neglect of the damping of asymmetry as the moving bubble surface generates a shock wave may also cause the effect of asymmetries to be overestimated. The results given here should therefore be considered a ''worst case'' analysis. We can say with some certainty that for bubbles with asymmetry less than one part in twenty, shock instability does not limit the temperatures reached at the center of the bubble.

[1] A.J. Walton and G.T. Reynolds, Adv. Phys. **33**, 595 (1984).
[2] S.J. Putterman, Sci. Am. **272** (2), (1995).
[3] R.A. Hiller and S.J. Putterman, Phys. Rev. Lett. **75**, 3549 (1995).
[4] B.P. Barber, K. Weninger, R. Lofstedt, and S.J. Putterman, Phys. Rev. Lett. **74**, 5276 (1995).
[5] R. Hiller, S.J. Putterman, and B.P. Barber, Phys. Rev. Lett. **69**, 1182 (1992).
[6] R. Hiller, K. Weninger, S.J. Putterman, and B.P. Barber, Science **266**, 248 (1994).
[7] B.P. Barber, C.C. Wu, R. Lofstedt, P.H. Roberts, and S.J. Putterman, Phys. Rev. Lett. **72**, 1380 (1992).
[8] C. Eberlein, Phys. Rev. A **53**, 2772 (1996).
[9] H.P. Greenspan and A. Nadim, Phys. Fluids A **5**, 1065 (1993).
[10] R. Lofstedt, B.P. Barber, and S.J. Putterman, Phys. Fluids A **5**, 2911 (1993).
[11] C.C. Wu and P.H. Roberts, Proc. R. Soc. London Ser. A **445**, 323 (1994).
[12] L. Kondic, J.I. Gersten, and C. Yuan, Phys. Rev. E **52**, 4976 (1995).
[13] H.-Y. Kwak and H. Yang, J. Phys. Soc. Jpn. **6**, 1980 (1995).
[14] M.P. Brenner, D. Lohse, and T.F. Dupont, Phys. Rev. Lett. **75**, 954 (1995).
[15] M.P. Brenner, D. Lohse, D. Oxtoby, and T.F. Dupont, Phys. Rev. Lett. **76**, 1158 (1996).
[16] T.J. Matula, R.A. Roy, P.D. Mourad, W.B. McNamara, and K.S. Suslick, Phys. Rev. Lett. **75**, 2602 (1995).
[17] R. Lofstedt, K. Weninger, S.J. Putterman, and B.P. Barber, Phys. Rev. E **51**, 4400 (1995).
[18] G.B. Whitham, *Linear and Non-linear Waves* (Wiley, New York, 1974).
[19] J.H. Gardner, D.L. Brook, and I.B. Bernstein, J. Fluid Mech. **114**, 41 (1982).
[20] D.W. Schwendeman and G.B. Whitham, Proc. R. Soc. London Ser. A **413**, 297 (1987).
[21] D.W. Schwendeman, Proc. R. Soc. London Ser. A **441**, 331 (1993).
[22] L.D. Landau and E.M. Lifshitz, *Statistical Physics*, 3rd ed. (Pergamon, Oxford, 1980) Pt. I.
[23] G.B. Whitham, J. Fluid. Mech. **2**, 146 (1957).
[24] G.B. Whitham, J. Fluid. Mech. **5**, 369 (1959).
[25] G. Guderley, Luftfahrtforschung **19**, 302 (1942).
[26] *Handbook of Mathematical Functions*, edited by M. Abramowitz and I.A. Stegun (Dover, New York, 1965).
[27] G. Birkhoff, Q. Appl. Math. **12**, 306 (1954).
[28] S.J. Putterman (private communication).